The Effects of Aberrations (Low Order and Quilting) on the Performance of the All-Composite Design for the Herschel Space Observatory

Brian Catanzaro[*a], James A. Thomas[b*], Stan Backovsky[c], Dan Barber[b], Don Small[b], Roger Johnston[b] and Eri Cohen[d]

[a]CFE Services, 5147 Pacifica Dr, San Diego, CA 92109
[b]Light Works Optics, Inc., 2691 Richter Ave., Suite 105, Irvine CA 92606
[c]Composite Optics Incorporated, 9617 Distribution Ave, San Diego, CA 92121
[d] Jet Propulsion Laboratory, California Institute of Technology,
4800 Oak Grove Drive, Pasadena CA 91109

ABSTRACT

The effects of specific aberrations on the optical performance of the all-composite design for the Herschel Space Observatory are examined. A review of the all-composite design for the large aperture (3.5 m) telescope that satisfies the target specifications is presented. Cyrogenic experiments with a carbon fiber reinforced polymer (CFRP) 2 m demonstration mirror have yielded empirical bounds on the high- and low-order spatial frequency aberrations that will be anticipated in the full 3.5 m Ritchey-Chretien telescope design. Detailed analysis is presented on the effect of the low order aberrations of the primary mirror on the system wavefront error and encircled energy. Predictable limits of correction via low order shaping of the secondary mirror are described. The impact of higher order surface errors on the encircled energy and the stray light will also be presented. Comments are made regarding the impact of the optical prescription and CRFP design on flight telescope testing.

Keywords: Carbon Fiber Composite, Space Telescope, PSF, Quilting, Cryogenic Telescope, Far Infrared, Low Spatial Frequency Errors, High Spatial Frequency Errors, Encircled Energy

1. INTRODUCTION

The Herschel Space Observatory (formerly known as FIRST), is a European Space Agency (ESA) cornerstone mission, that will be used for photometry, imaging and spectroscopy in the 80 to 670 μm range (see Figure 1). The key science goals that this observatory will achieve concern how galaxies formed in the early universe, and how stars form, and have been forming, throughout the history of the universe. NASA, through the Jet Propulsion Laboratory (JPL), has contributed to the telescope and its design. [1] This paper will discuss the work done by JPL, Composite Optics, Incorporated (COI), and Light Works Optics, Incorporated (LWO) in an effort to demonstrate the compliance of a carbon fiber composite telescope with the requirements for the Herschel Space Observatory.

* Correspondence: Email: bcatanza@alumni.caltech.edu; Telephone: 858 204 6299;

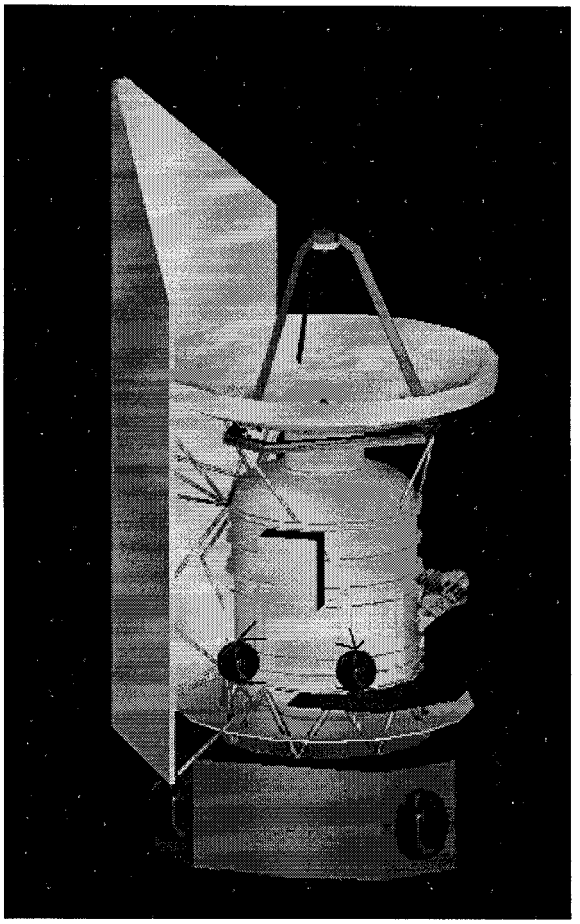

Figure 1: Herschel Space Observatory

The design proposed by COI and JPL (see Figure 2) consisted of a carbon fiber composite primary mirror, a carbon fiber composite tripod, and a zerodur secondary mirror. The primary mirror was designed as a sandwich mirror using a unique process of molding facesheets and precision assembly; the mirror itself would never be polished, however the mold and assembly fixture would be polished. [2] The design for the facesheet consisted of six (6) independent panels arranged as sectors of a circle. Ribs provide a sparse core that provides support between the facesheets and connects the facesheets to the backsheets. The secondary mirror was to be figured to match and correct for low order aberrations in the primary mirror. In order to verify this design, a 2 m demonstration mirror was fabricated (see Figure 3) and tested at cryogenic temperature. [3]

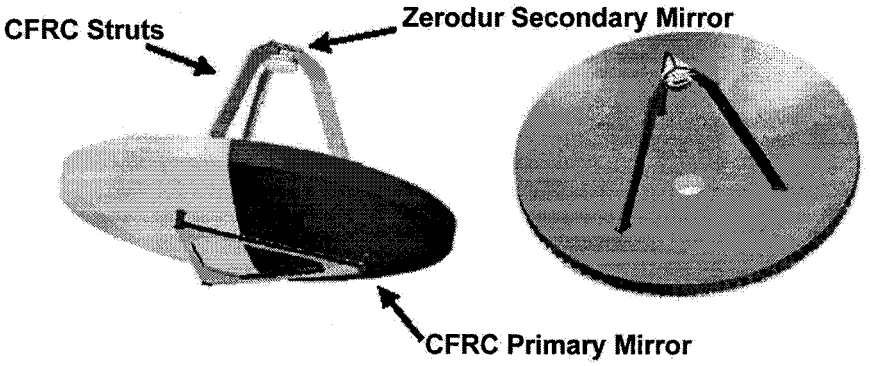

Figure 2: Carbon Fiber Composite Telescope Design

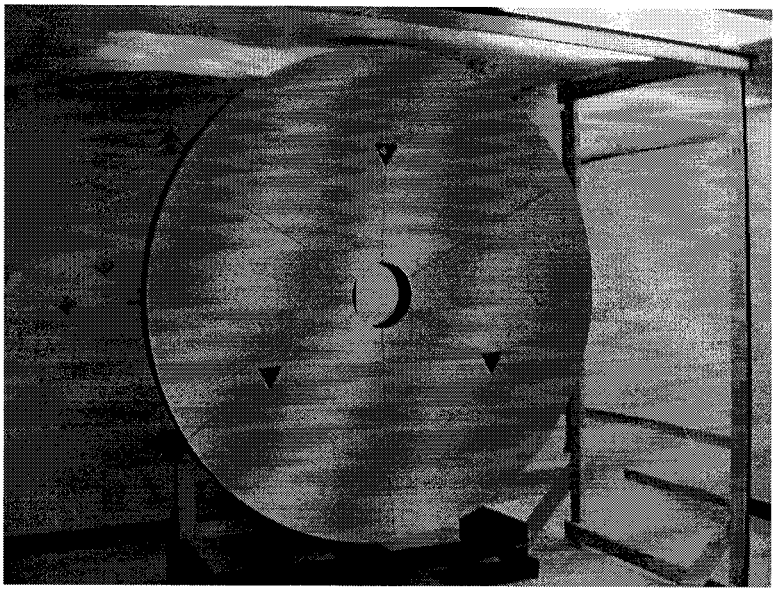

Figure 3: 2 m Diameter Demonstration Mirror

The demonstration mirror fabricated to reduce risk in the design is a 2 m diameter, F/1 spherical mirror. The mirror is coated with a protected gold reflective layer. The mirror was fabricated using the same methodology planned for the flight telescope.

Presented here is a review of the telescope design and requirements. This is followed by a summary of the low order errors measured from the 2 m demonstration mirror. The correction factor afforded by figuring the secondary mirror is discussed. Next, the impact of the residual low order errors on the telescope performance is described. The measurement data for high order errors is then described. Following this is the impact these errors have on telescope performance and the flight telescope test.

2. TELESCOPE DESIGN

The telescope optical prescription is summarized in Table 1. The telescope has a large, fast primary mirror that although it is technically hyperbolic, is very close to parabolic. The secondary mirror will be figured as an arbitrary asphere to correct for low order aberrations in the primary mirror. The image plane is parabolic.

Table 1: Telescope Prescription

Element	Parameter	Value
Primary Mirror	Clear Aperture	3.5 m
	Radius of Curvature	3.5 m
	Conic Constant	-1.001289
Secondary Mirror	Clear Aperture	0.3083 m
	Radius of Curvature	0.3453 m
	Conic Constant	-1.296000
Focal Surface	Clear Aperture	0.245 m
	Radius of Curvature	0.1672 m
	Conic Constant	-1.0
Despace		1.58797 m
Primary Mirror Vertex to Focus		1.05 m
EFL		28.5 m

A subset of the performance specifications for the Herschel Space Observatory is summarized in Table 2. There are several specifications for the Herschel Space Observatory related to stray light. Only the requirement related to interferometric measurements and the point spread function (PSF) will be discussed. Figure 4 illustrates the encircled energy specification.

Table 2: Herschel Space Observatory Performance Specifications

Parameter	Value
Wavefront Error	≤ 6 μm RMS
Encircled Energy	See Figure 4
Field of View (FOV)	±0.25 degrees
Stray Light	PSF < 10^{-4} at > 3'

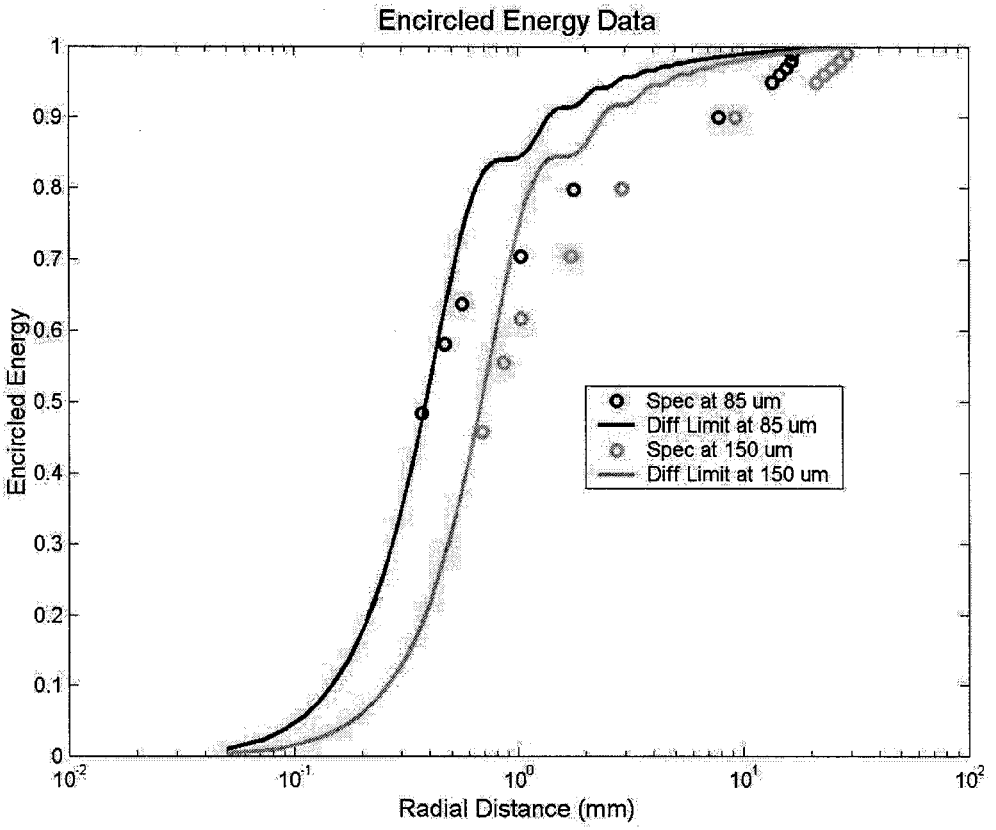

Figure 4: Encircled Energy Specification

3. MEASUREMENT DATA FOR LOW ORDER ERRORS

The low order errors in the demonstration mirror were characterized during a number of tests. These errors were reduced to Zernike coefficients. The first 36 terms were considered to be low order errors; correctable by figuring the secondary mirror. This data was then scaled to the telescope primary mirror.

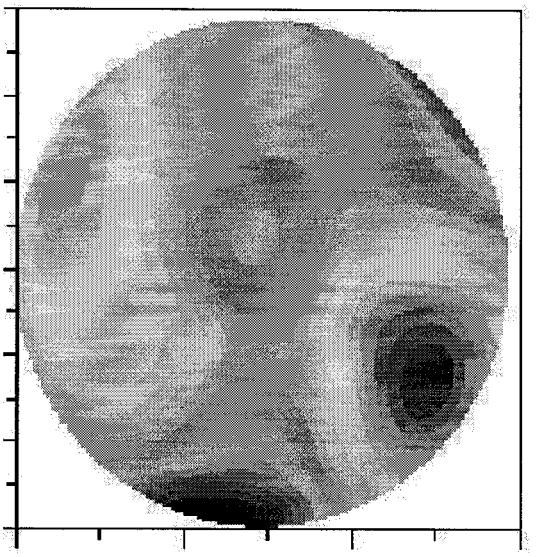

Figure 5: Low Order Zero Gravity Surface Map (Surface Error: 2.1/11.8 μm RMS/PV)

The characterization of the demonstration mirror included a zero gravity surface map and a cryogenic deformation surface map. The zero gravity surface map was generated by measuring the surface in three orientations and averaging the interferograms to nullify the effects of gravity. Zernike coefficients were calculated from this surface and a zero gravity surface was constructed (see Figure 5). The data shown in Figure 6 was the result of difference maps from room temperature and 70 K surface measurements. [3] Again, the first 36 Zernike coefficients were calculated and used to reconstruct a surface.

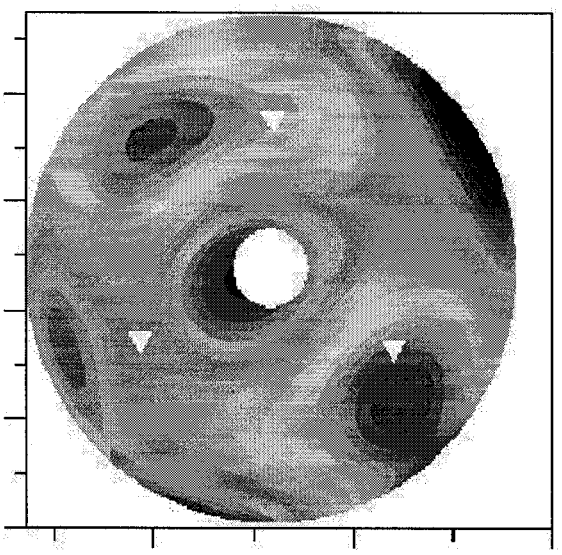

Figure 6: Low Order Cyrogenic Deformation (70 K) Surface Map (Surface Error: 3.4/15.4 μm RMS/PV)

Several methods were considered for extrapolating the figure to the flight telescope primary. The test data was measured over a 2 m aperture, yet the flight telescope will have a 3.5 m aperture. One would expect the low order error to be different in the larger flight mirror. One method for scaling is to multiply the existing data from the 2 m demonstration mirror by a constant factor to capture a worst case scenario. Alternate scaling laws have been used for polished mirrors. One approach is to use empirical power laws to scale each of the Zernike coefficients with diameter. Another approach is to use the

coefficients from the 2 m demonstration mirror measurements and allow the Zernike polynomials to continue beyond the unity circle to the 3.5 m diameter. Recall that the construction of the primary mirror was not based on polishing a 3.5 m mirror. As such, these historical scaling laws from polished mirror heritage may not be representative. Heritage from COI reflectors built with similar construction techniques have not demonstrated significant changes in RMS and peak to valley deformation with increase in size. Another scaling method is to use finite element analysis (FEA) to predict the behavior of effects thought to impact fabrication accuracy. The FEA was performed with both conservative and aggressive assumptions, producing two different mirror shapes in order to bound the prediction between a best case and worst case scenario. Figure 7 shows two examples of the flight telescope primary mirror prior to correction. On the left is an example of using the 2 m demonstration mirror data without scaling. On the right is an example of adding the zero-gravity test data and the 3.5 m FEA data.

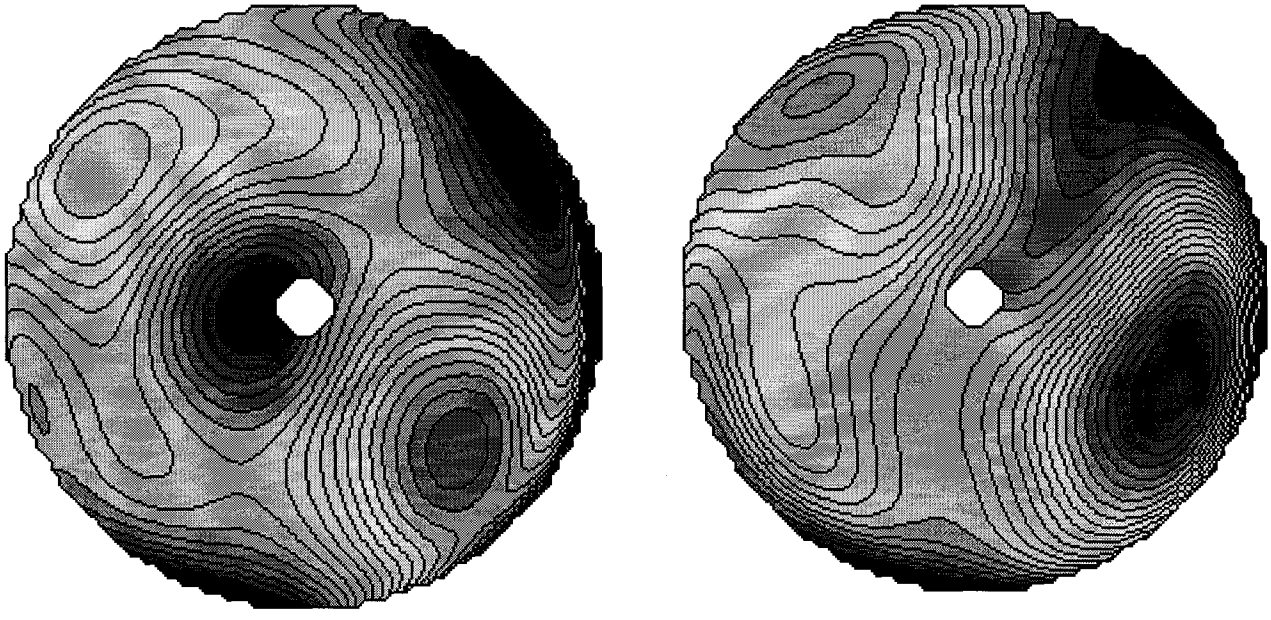

Zero-G Surface + Delta to Cryo Data: 293K to 70K

11 μm RMS

Zero-G Surface + FEA

9.0 mm RMS

Figure 7: Low Order Representations of the 3.5 m Primary Mirror for the Flight Telescope

4. CORRECTABILITY WITH SECONDARY MIRROR

The secondary mirror will be used to correct aberrations in the primary mirror. In this design the correction is limited by the field of view not by the fabrication technology. A complete ray tracing analysis yields a more accurate correction function that achieves > 90% correction at extremely low spatial frequencies and little to no correction at higher spatial frequencies.

An intuitive model for understanding this effect is based on nulling out defects in the primary by making a reduced map of the primary mirror's aberrations on the secondary mirror. Using this intuitive model, an upper limit on the spatial frequencies that can be corrected can be derived from the field of view. At the center of the field of view, the aberrations from the primary mirror are mapped to the center region of the secondary mirror. At the edge of the field of view, these aberrations are shifted by:

$$\delta_2 = D_{12}\theta_{FOV},$$

where θ_{FOV} is the half angle of the field of view, D_{12} is the spacing between the primary and secondary mirror, and δ_2 is the shift. This can be projected back to the primary mirror by using the magnification between the primary and secondary mirrors:

$$\delta_1 = D_{12}\theta_{FOV}\frac{\phi_1}{\phi_2},$$

where δ_1 is the shift, and ϕ_1 and ϕ_2 are the diameters of the primary and secondary mirrors respectively. This quantity, δ_1, is the smallest feature that can be corrected by the secondary mirror. For this telescope design, the value is $\delta_1 = 81$ mm. This indicates that features below this size cannot be corrected across the field. For features larger than this size a relationship between the correction efficiency and the size of a feature can be established.

An analytical model can lend insight into the relationship between defect size, field of view, and correction efficiency. Using a simple conceptual model of a square defect (hill or valley) on the primary mirror, the RMS can be calculated:

$$W_\sigma = \phi\sqrt{\frac{s^2}{A}(1-\frac{s^2}{A})},$$

where A is the area of the mirror, s is the size of the square defect, and ϕ is the height of the defect. Nominally, the secondary mirror can be used to correct this defect for a single field point (e.g. on-axis). However, for off-axis field points, the correction on the secondary mirror will be misaligned with respect to the defect on the primary mirror. Using the square defect model, an expression for the RMS of the corrected wavefront as a function of a misalignment can be created:

$$W_\sigma' = \phi\sqrt{\frac{2\varepsilon \times s}{A}},$$

where ε is the error in aligning the correction to the primary mirror. By setting the error to the shift anticipated due to the field of view of the telescope and comparing the two expressions for RMS, a correction efficiency can be established:

$$\eta = \frac{W_\sigma'}{W_\sigma} = \sqrt{\frac{2\varepsilon}{s}\times\frac{1}{(1-\frac{s^2}{A})}}.$$

By setting the efficiency to 50% and ε to δ_1, the minimum size feature that can be corrected is 660 mm or 2.5 cycles across the primary mirror. Using this approximate model, features smaller than this will have little to no correction, features larger than this are anticipated to be very well corrected. Bear in mind that as the defect size, s, decreases, the overall contribution to the RMS decreases. As such the emphasis should be on correcting large features, not small ones.

A variety of scaled representations of the 3.5 m mirror were used as input to a ray tracing analysis. A merit function for optimization was established based on combining the wavefront errors from various field points across the ±0.25° field of view. The secondary mirror was adjusted by optimizing its aspheric coefficients to minimize this merit function. Although the edge of the field was the most difficult to optimize, the percentage reduction in RMS error was almost linear with respect to the magnitude of the RMS error of the primary mirror. The actual correction efficiency was calculated and features roughly 320 mm in size were corrected with better than 50% efficiency. The correctability on-axis was in excess of 95% and the correctability at the edge of field was no worse than 80%.

5. LOW ORDER ERROR IMPACT ON PERFORMANCE

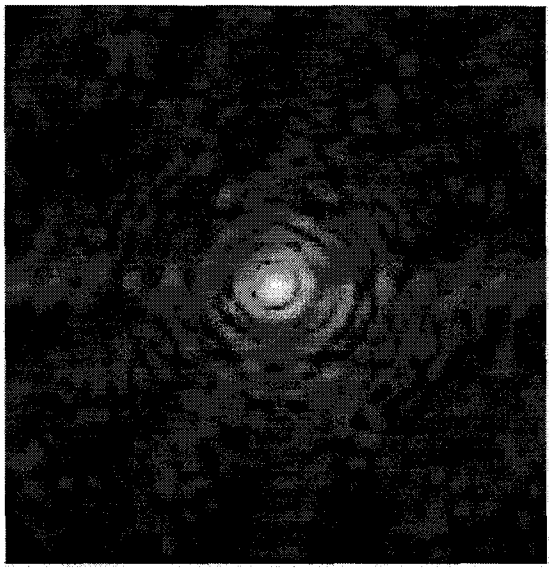

Figure 8: PSF Predicted for Telescope After Correction with the Secondary Mirror

Low order errors in the wavefront of the telescope have an impact on the wavefront error requirement and the encircled energy. Using the scaled representation of the 3.5 m primary mirror, the PSF for the telescope can be generated. Figure 8 shows an example of a PSF (λ = 85 μm) for the scaled representation of the FEA data (worst case) after correction by the secondary mirror.

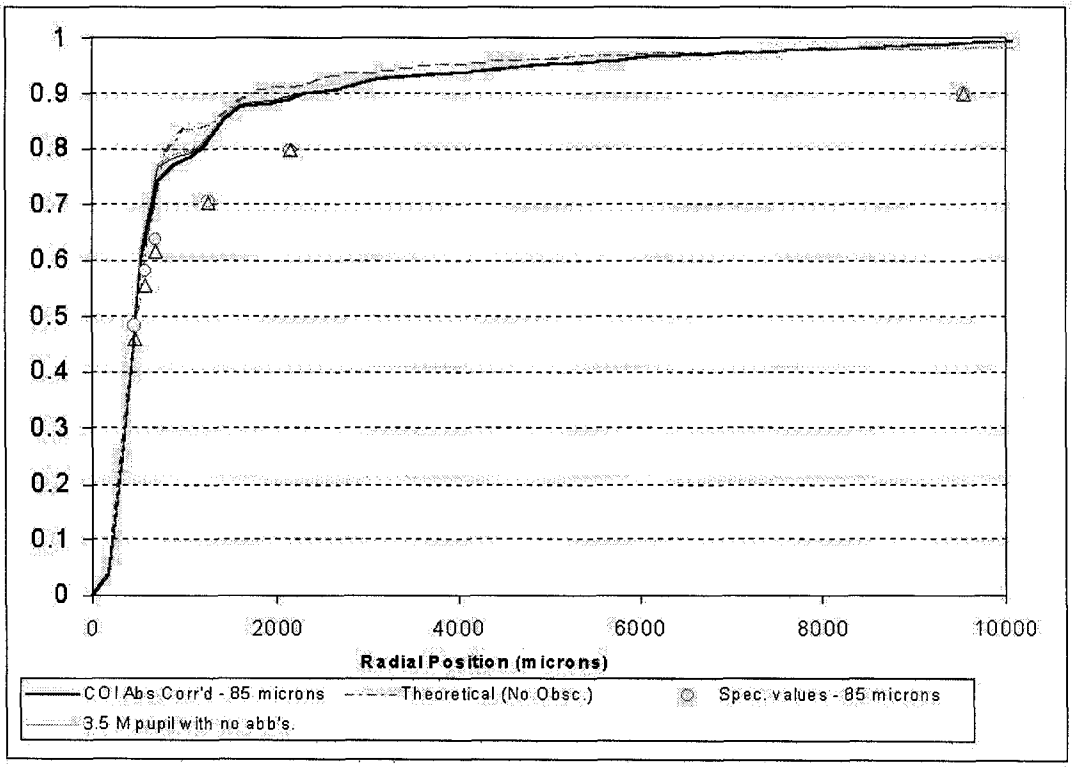

Figure 9: Encircled Energy of Corrected Telescope Wavefront Error

Once the primary mirror has been corrected by the secondary mirror the effect of the residual wavefront error (< λ/10 RMS) on the encircled energy is almost negligible. It is commonly assumed that diffraction limited wavefronts of λ/10 or less demonstrate little impact on the Strehl ratio, but the distribution of these errors among the first set of Zernike terms can have a large impact on encircled energy. However, the nature of the correction from the secondary mirror and the relatively small high order errors for this telescope cause little deviation from the diffraction limited encircled energy. Generally, the encircled energy specification is not as restrictive as the wavefront error specification. Figure 9 shows the encircled energy requirements (circular markers) compared to the prediction (based on scaled data) and the diffraction limit (dashed).

6. MEASUREMENT DATA FOR HIGH ORDER ERRORS

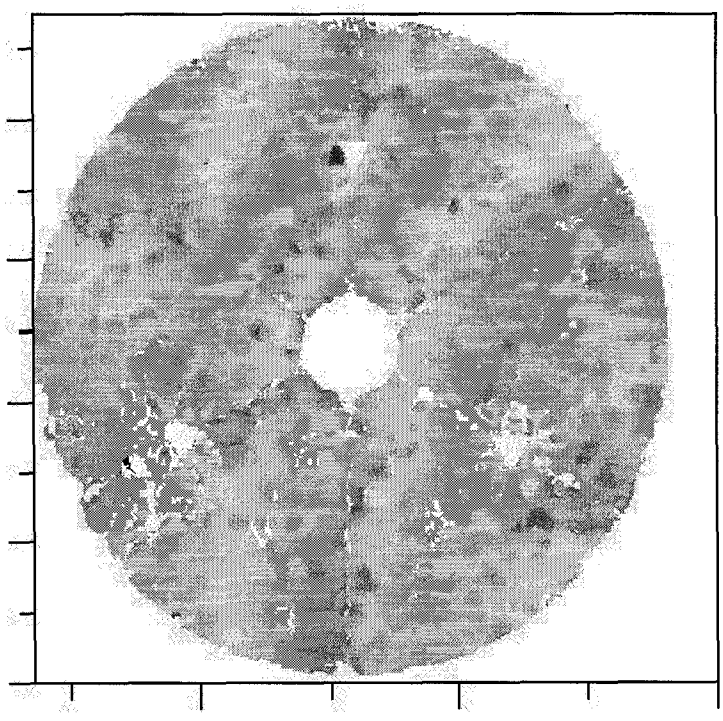

Figure 10: High Order Representation of the 2 m Mirror at 70K (Surface Error: 1.9/20 μm RMS/PV)

As described previously, some errors will remain after correction by the secondary mirror. These errors are primarily high order errors of frequencies higher than 5 cycles across the primary mirror. These errors are generally due to quilting from the rib support structure. Figure 10 shows the high order errors from the 2 m demonstration mirror. The geometry and material properties that govern quilting (rib geometry, facesheet thickness, material variability) are not expected to scale with diameter and therefore the quilting in the 3.5 m flight mirror is anticipated to be similar to the 2 m demonstration mirror test data.

7. HIGH ORDER ERROR IMPACT ON TELESCOPE PERFORMANCE

High order errors are anticipated to effect all four of the aforementioned specifications:

- Wavefront Error,
- Encircled Energy,
- Stray Light inside the FOV

The effect on wavefront error is straightforward. The RMS residual surface error is added to the surface error budget and added using root sum squared (RSS) approach. The contribution from high order errors is: 1.9 μm RMS surface error.

The effect of higher order aberrations on encircled energy is driven in this case by quilting. Quilting can be considered in the worst case as a periodic structure. Concentric rings have been modeled. [4] When modeled in this fashion, the period determines the distance of the side lobes from the PSF peak and the amplitude of the quilting determines the amplitude of the side lobes. The distance of the side lobes from the center of the PSF is given roughly by:

$$\theta_n = \frac{n\lambda}{\Lambda_g},$$

where θ_n is the distance of the n^{th} side lobe in radians, n is the diffraction order, Λ_g is the period of the quilting, and λ is the wavelength of use. The amplitude of the side lobes is given by:

$$I_n = 2\frac{J_n(A_{PV}k)^2}{nDK_g}, \quad k = \frac{2\pi}{\lambda}, K_g = \frac{2\pi}{\Lambda_g}$$

where A_{PV} is the peak to valley of the quilting and D is the diameter of the primary mirror. In this model, the reduction in Strehl ratio is merely:

$$J_0(A_{PV}k)^2.$$

For quilting errors with less than 5.2 μm peak to valley wavefront error (2.6 μm peak to valley surface error), the reduction in the Strehl ratio at λ = 85 μm is approximately 7.2%. This is a minor impact to the encircled energy.

Table 3: Specification Compared to Scattering Angles (λ = 85 μm)

Parameter	Radial Distance from PSF Peak (Airy Diameters)	Radial Angle
FOV	69	4.400 mrad
Enc. Energy	< 9	0.580 mrad
Stray Light	> 14	0.870 mrad
Rib Quilting	13	0.810 mrad

The stray light specification on the PSF (point spread function) requires that the value of the PSF drop to 10^{-4} outside of 3 arc minutes from the peak. High order quilting has an impact on this specification based on the frequency of the quilting. By using Fourier optics, it is straightforward to calculate the angle of scatter of the triangular quilting features (see Table 3). The angle can be expressed in terms of Airy disc diameters rather than angle. The diffraction limit of the telescope at 85 μm is 0.063 mrad (one Airy diameter). The field of view of the telescope is 69 Airy diameters (±0.25° or ±4.4 mrad). The encircled energy specification covers out to 9 Airy diameters (±16.7 mm or ±0.58 mrad). The 3 arc minute (0.87 mrad) specification is equivalent to 14 Airy diameters. For calculation purposes, the rib spacing (the primary cause of quilting) is approximately 0.105 m or 13 Airy diameters. Therefore the first side lobe from quilting falls close to the 3 arc minute requirement and many of the higher orders would fall in the region from 3 arc minutes to the edge of the field of view.

A specific study performed by TICRA [5] computed the effects of quilting based on a quadratic phase applied with an isogrid pattern across the mirror face. This study assumed a 2 μm peak to valley error. The largest side lobe was -32 dB (6.3×10^{-4}). However, this was inside the 14 Airy diameter lower limit for stray light. The largest side lobe relevant to the stray light specification was -36 dB (2.5×10^{-4}).

The PSF can be calculated numerically from the data collected from the 2 m demonstration mirror. Although the 2 m demonstration mirror is smaller than the primary mirror of the telescope, it can be shown that the calculated PSF is adequate for demonstrating compliance with the specification. Consider that a quilting phase function exists for the mirror and the wavefront from the mirror can be expressed as:

$$W_{mirror}(r) = circ(\frac{r}{R_0})\exp(\iota\phi_q),$$

where R_0 is the radius of the aperture of the mirror and ϕ_q is the quilting function. The PSF is the Fourier transform of the wavefront (W_{mirror}) normalized such that at the center the value is 1. This corresponds to dividing the Fourier transform of the wavefront by the area of the aperture. This can also be expressed as the convolution of the unaberrated (non-quilted) wavefront with the Fourier transform of the quilting function:

$$PSF = \frac{F.T.\{W_{mirror}(r)\}}{\pi R_0^{\,2}} = \frac{F.T.\left\{circ(\frac{r}{R_0})\right\}}{\pi R_0^{\,2}} * F.T.\{\exp(\iota\phi_q)\}$$

The quilting is assumed to be periodic in nature. As such, the Fourier transform is anticipated to contain a series of spikes or peaks. As shown earlier, some of these peaks should occur inside the stray light specification (14 Airy diameters). These peaks can be approximated as Dirac delta functions in which case, the PSF can be re-written as:

$$PSF = \frac{F.T.\left\{circ(\frac{r}{R_0})\right\}}{\pi R_0^{\,2}} * \sum_i C_i \delta(\vec{\rho} - \vec{\rho}_i) = \frac{\left(J_1(2\pi\rho R_0)/\rho R_0\right) R_0^{\,2}}{\pi R_0^{\,2}} * \sum_i C_i \delta(\vec{\rho} - \vec{\rho}_i),$$

$$PSF = \frac{J_1(2\pi\rho R_0)}{\pi\rho R_0} * \sum_i C_i \delta(\vec{\rho} - \vec{\rho}_i),$$

where ρ is the radial spatial frequency.

This convolution creates copies of the unaberrated PSF at each of the quilting locations in proportion with their weighting, C_i. Generally, since the features creating the quilting are much smaller than the size of the mirror aperture, the corresponding peaks in the PSF are separated by a large amount. As a consequence, there is little to no interaction between each of the peaks. Therefore, each peak can be considered individually as:

$$Peak_i = C_i \left.\frac{J_1(2\pi\rho R_0)}{\pi\rho R_0}\right|_{\rho=0} \text{ shifted to location } \vec{\rho}_i$$

The height of these peaks is merely the weighting function multiplied by the unaberrated PSF evaluated at $\rho = 0$. The unaberrated PSF (sometimes referred to as a Jinc function) is normalized to unity. Therefore the height of the peaks is merely C_i which is independent of the size of the aperture. Although the size of the aperture will cause these peaks to change width (larger aperture will narrow the peaks), it will not cause the height of the peak to change.

With this understanding, the PSF can be evaluated with the quilted 2 m demonstration mirror data. If the values for this numerical computation of the PSF meets the specification (no value larger than 1×10^{-4}), and if the same quilting function exists on the 3.5 m primary mirror, then it too will meet the specification (recall that the rib spacing will not change so assuming the amplitude and shape are represented by the 2 m demonstration mirror, this assumption is valid).

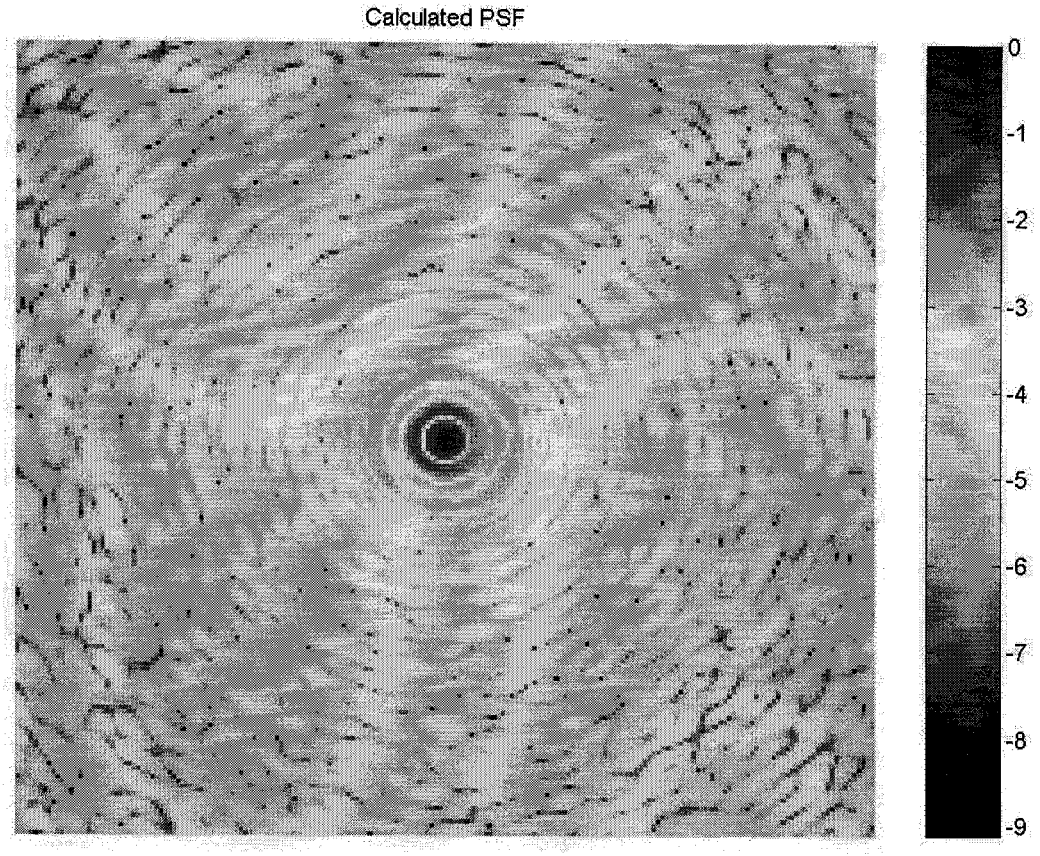

Figure 11: Calculated PSF for 2 m Demonstration Mirror - Logarithmic Scale

In order to evaluate the effect of quilting on the PSF properly, the unaberrated (diffraction limited) PSF was first calculated. Then the aberrated (quilted) PSF was calculated (see Figure 11). The two were differenced to create the residual PSF which represents the effect of quilting. The values of interest in this residual PSF are those that are greater than the stray light limit (14 Airy diameters) and less than the Field of View (69 Airy diameters). This annulus is shown in Figure 12. The largest value is 0.28×10^{-4}. Two features are noteworthy. First, the values are all below the specification (1×10^{-4}) and second, there are no periodic peaks. The lack of periodic peaks indicates that although there is quilting in the mirror, it is not highly periodic.

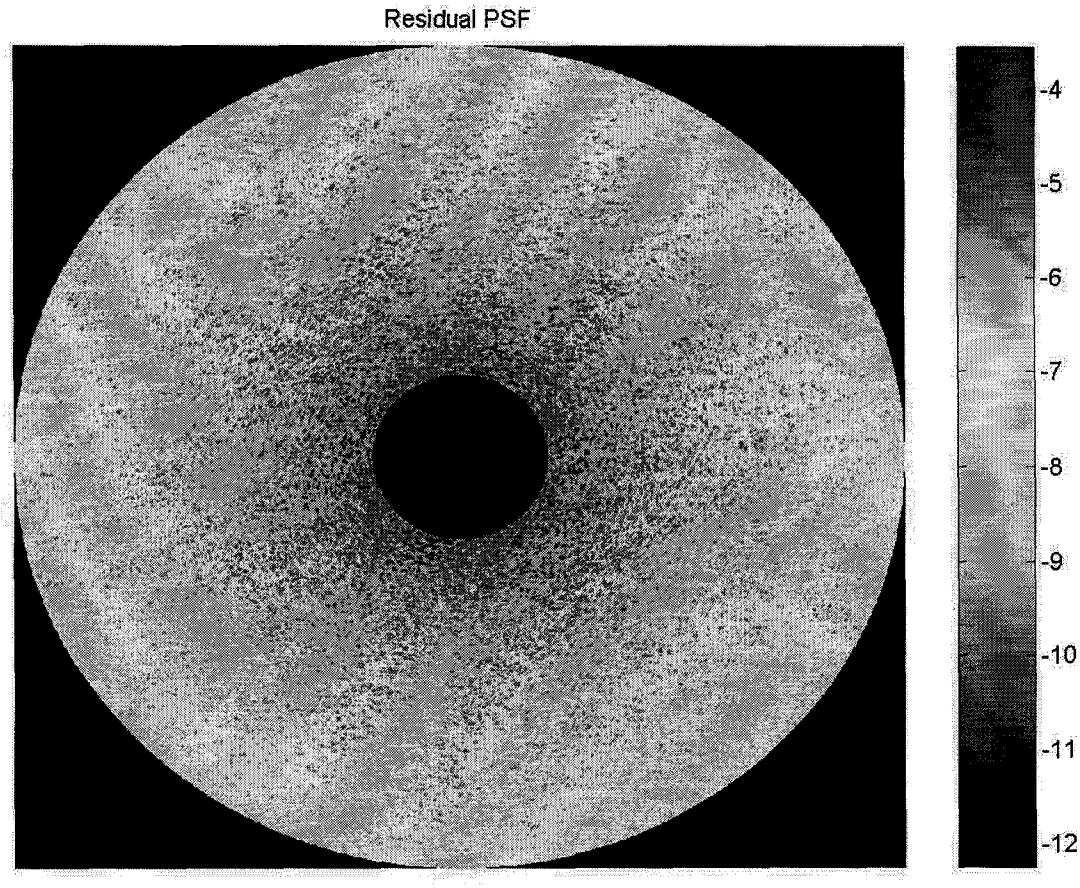

Figure 12: Effect of Quilting PSF for 2 m Demonstration Mirror - Logarithmic Scale (Only the Region Beyond the Stray Light Limit and Inside the FOV is Shown).

8. IMPLICATIONS FOR FLIGHT TELESCOPE TESTING

The telescope design and data from the 2 m demonstration mirror have certain implications on the testing of the flight telescope.

The operational temperature and size of the primary mirror of the Herschel Space Observatory place significant constraints on flight testing the optical performance of the telescope. The operational temperature of 90 K – 70 K suggests that the test should be performed in a thermal vacuum chamber that is at least liquid nitrogen capable and hopefully gaseous helium cooled. With liquid nitrogen only, the telescope will not reach the 70 K lower limit of the operational range. Even if the requirement for testing was relaxed to 90 K and if a series of custom shrouds and cold straps were used, the gradients would not drop below an acceptable amount until after a very long stabilization period. Therefore, the test environment should be capable of at least gaseous helium cooling. Given the challenges of custom shroud(s) and the optical test, it is unlikely that a separate test for the primary mirror and the integrated telescope is practical. It is more efficient to test the telescope in a fashion that provides alignment data and/or aspheric figuring data for the secondary mirror. The size of the primary mirror (3.5 m) also places constraints on the test. Many smaller telescopes of this type have been tested using a precision optical flat equal in size to the primary. The flat may be warm or cold depending on its construction, the chamber, and the thermal management of the telescope. However, the construction of a flat 3.5 m in size is an expensive and time-consuming task. Were such a flat to be constructed, other issues of testing the flat, transporting it, and mounting it in the chamber would arise. One approach to surmounting these problems is a sub-aperture test.

A sub-aperture test would entail a moveable, smaller (nominally 1 m) flat capable of optically testing several overlapping sections of the telescope (see Figure 13). Interferometric data would be collected at each position of the moveable flat. The

data would then be used to reconstruct a full aperture wavefront using stitching techniques. [6] Generally the flat should be large enough to minimize the number of overlapping sections but small enough to gain the advantages of cost and thermal loading.

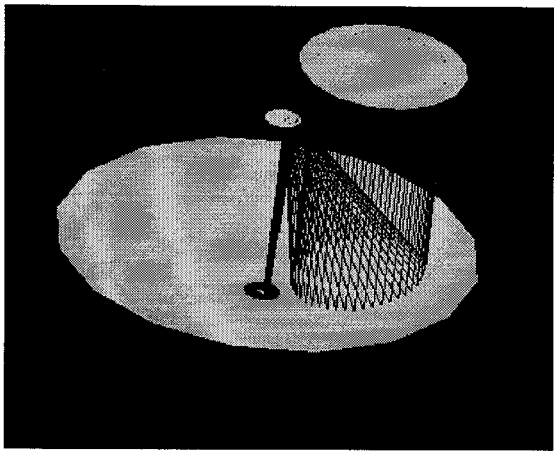

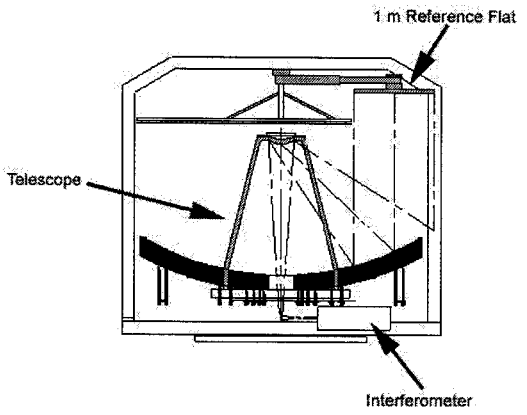

Ray Trace of Sub-Aperture Test Concept **Schematic of Sub-Aperture Test Concept**

Figure 13: Sub-Aperture Test Concept

Using the data collected from the 2 m demonstration mirror the sub-aperture testing approach can be explored. Sub-aperture data was collected on the 2 m demonstration mirror at various temperatures including 70 K. This data was used to reconstruct a full aperture map of the surface. This "stitched" surface was then compared with the full aperture map. The low order figure match was between 0.5 μm and 1.8 μm RMS depending on the technique used to reconstruct the surface. [6] The full aperture (non-stitched) data was separately scaled to a 3.5 m size to further simulate sub-aperture testing of the flight telescope. A ray-tracing model of the sub-aperture test was created and interferograms for $\lambda = 10.6$ μm were simulated. (see Figure 14) The slope errors encountered were similar to those measured during the 2 m demonstration mirror test. This suggests that high fidelity wavefront data can be collected from the flight telescope using a 1 m flat.

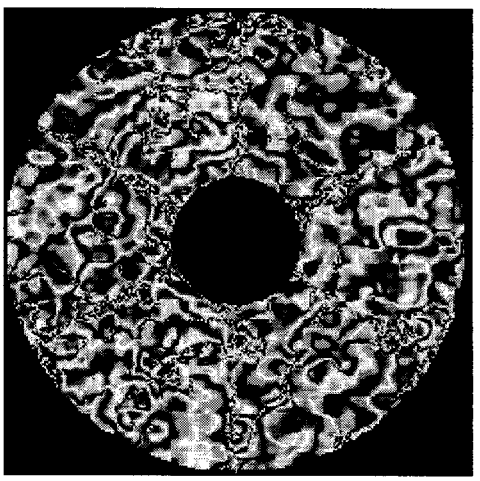

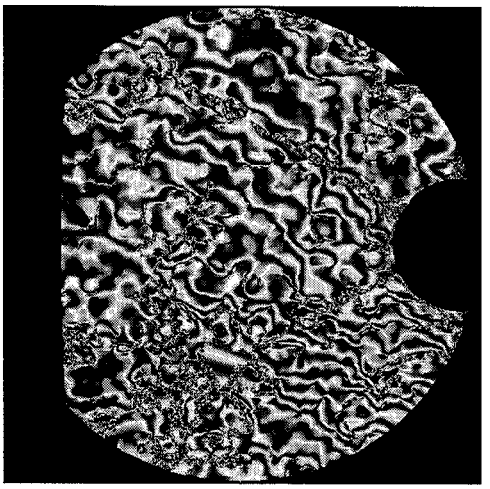

Centered 1 m Flat **Off-Axis 1 m Flat**

Figure 14: Simulated Interferograms from a Ray Tracing Model of the Sub-Aperture Test Concept

9. SUMMARY

A CFRP telescope meeting the specifications for the Herschel Space Observatory has been described. The telescope includes a secondary mirror, aspherically figured to remove aberrations generated by a lightweight CFRP primary mirror. Experimental data from a crygonically tested 2 m demonstration mirror has been presented. This data has been interpreted in the context of the specifications for the Herschel Space Observatory using low and high order figure data. The data supports the CFRP telescope design by demonstrating compliance with wavefront error, encircled energy, and stray light specifications. Finally, comments are made regarding the implications of the design of the telescope on optical testing. Sub-aperture testing has been suggested as an alternative to a full aperture test.

10. ACKNOWLEDGEMENTS

The work described in this paper was carried out by COI, LWO and JPL (California Institute of Technology), under a contract with the National Aeronautics and Space Administration.

11. REFERENCES

1. E. J. Cohen, S. J. Connell, K. J. Dodson, J. L. Abbot, A. Abusafieh, Z. Backovsky, J. Dyer, J. Escobedo-Torres, Z. Friedman, A. Hull, D. Small, P. Thorndyke, and S. Whitmore "Architecture of the FIRST telescope," SPIE Proceedings Vol 4015, March 2000.
2. S. J. Connell, K. J. Dodson, Z. Friedman, B. Catanzaro, S. Whitmore, and E. J. Cohen "Design progression of an all-composite primary mirror for the FIRST Telescope," SPIE Proceedings Vol 4013, March 2000.
3. B. Catanzaro, S. Connell, M. Mimovich, Z. Backovsky, G. Williams, J. A. Thomas, D. Barber, R. Johnston, J. Hylton, K. Dodson, and E. Cohen "Cryogenic (70K) measurement of an all-composite 2-meter diameter mirror," SPIE Proceedings Vol 4444, Aug 2001.
4. Applied Optics and Optical Engineering Vol VIII, Chapter 6 (W. Wetherell), R. Shannon and J. Wyant (eds.), Academic Press.
5. H. Nielson "RF effect of core print-through distortion on the FIRST telescope," TICRA engineering consultants, May 2000.
6. B. Catanzaro, J. A. Thomas, and E. J. Cohen "Comparison of full-aperture interferometry to sub-aperture stitched interferometry for a large diameter fast mirror," SPIE Proceedings Vol 4444, August 2001.